https://doi.org/10.3311/PPci.40555



**Periodica Polytechnica Civil Engineering**, 69(4), pp. 1321–1332, 2025

# Durability Indices of a Sealing Mortar Incorporating Blast Furnace Slag

## Comparison with a Commercial Reference

Soumia Ikhaddalene[1*], Amar Irekti[1], Mehena Oualit[1]

[1] Laboratory of Applied Chemistry and Materials (LabCAM), Chemistry Departement, Faculty of Science, University of M'hamed Bougara of Boumerdes, Avenue de l'Indépendance, 35000 Boumerdes, Algeria
[*] Corresponding author, e-mail: iksoumia@univ-boumerdes.dz

Received: 27 March 2025, Accepted: 02 October 2025, Published online: 30 October 2025

**Abstract**

Ground granulated blast furnace slag generated from steel manufacturing presents environmental challenges, but it can be valuable when utilized as a supplementary material in concrete, contributing to the development of sustainable materials. In this research, a new sealing mortar was prepared by substituting 10% of the cement with slag (M10). This material can provide performance comparable to M234, a M0 sealer used for sealing and wedging supports and machine bases. The mechanical properties and durability indices of both M10 and M234 were compared to the reference mortar MISO, which is a laboratory-made mortar free of slag. XRD analysis was conducted to determine the crystallinity of the starting cement, and granulometry revealed a median size distribution of 23 μm for the slag after grinding. Capillary absorption and water-accessible porosity were tested for all samples.

**Keywords**

sustainable material, substitution, sealing mortar, mechanical properties, durability

### 1 Introduction

Slag produced in steelmaking operations is generally classified into three primary types, corresponding to the furnace in which it is generated: basic oxygen furnace (BOF) slag, electric arc furnace (EAF) slag, and ladle furnace (LF) slag [1, 2]. Compared to BOF slag, EAF and LF slags are less reactive and alkaline, making them potentially useful materials [3–5].

The cooling mechanism of the slag determines its two main types: ground glassy slag (vitrified) and crystallized slag. The first form contains either granulated or pelletized slag, while the second has a rock structure resulting from the slowest possible cooling process.

Ground Granulated Blast Furnace Slag (GGBS) is an industrial solid waste material generated during the manufacturing process of pig iron in the blast furnace [6, 7]. Additionally, its accumulation in landfills causes significant environmental problems; therefore, its valorization could lead to substantial environmental benefits and economic advantages. GGBS is primarily composed of calcium silicates and aluminosilicates, along with other bases that form in an igneous state with iron during this process [7, 8].

On the other hand, concrete is one of the most widely used man-made construction materials. Notably, it has the capacity to fully absorb alternative substances derived from industrial waste, contributing to sustainable development.

It was found that using GGBS in cement and concrete as a supplementary material can lead to significant cost savings [9, 10] and develop a sustainable material by enhancing certain properties of both fresh and hardened concrete, such as mechanical properties (compressive, flexural, and tensile strength) [11] durability, and thermal behavior [12–15].

The literature contains some interesting works on cementitious materials containing granulated slag [16–18]. For example, Monshi and Asgarani [19] worked with steel slag (at 8%) to prepare different types of cement. Their work suggests that slag should be used in small amounts when making cement to maintain the required strength and ensure a longer lifespan for the cement. In a similar context, Tsakiridis et al. [20] conducted a study on using steel slag in Portland cement and found that adding up to 10.5% granulated slag to the clinker did not negatively impact the quality of the produced cement. Another study led by Vejmelková et al. [21] presented a high-performance concrete containing 10% GGBS, which exhibited 20% less open porosity than conventional concrete,

**Cite this article as:** Ikhaddalene, S., Irekti, A., Oualit, M. "Durability Indices of a Sealing Mortar Incorporating Blast Furnace Slag: Comparison with a Commercial Reference", Periodica Polytechnica Civil Engineering, 69(4), pp. 1321–1332, 2025. https://doi.org/10.3311/PPci.40555

offering lower porosity and better durability than ordinary Portland cement concrete.

Wang et al. [22] studied the influence of a slightly higher content of steel slag replacement (45%) on the properties of concrete. They showed that this concrete exhibit lower early strength but higher late strength than pure cement concrete. Moreover, slag concrete can achieve a similar level of permeability, drying shrinkage, and carbonation resistance as pure cement concrete. Teng et al. [23] noted that increasing the surface area by using ultrafine GGBS in concrete (30%) results in higher early strength, lower permeability, and improved durability.

However, cementitious materials, such as concrete, are intrinsically porous, and their high fragility and low tensile strength make them sensitive to cracking under various environmental conditions. As a result, they are vulnerable to aggressive agents like chlorides, nitrates, and sodium, calcium, or magnesium sulfates present in water and aggressive fluids, which can eventually lead to physical and chemical degradation over time [24]. This degradation limits their lifespan and lowers their structural performance, potentially leading to costly repairs and failures.

Consequently, sealing mortar is a useful product that allows for the physical sealing of various structures. It can be used to seal cracks, joints, or stone structures [25], and it also prevents aggressive fluids from seeping into the mortar. This type of mortar can also be employed for wedging supports, machine bases, posts, and anchors.

For example, Issa and Debs [26] used epoxy resin to repair cracks in concrete through injection and gravity filling to restore its structural integrity, concluding that the properly applied epoxy system re-established compressive strength by up to 8.23%. Meanwhile, Abolfazli et al. [27] conducted a comparison between chemical grouting and cement grouting using epoxy and polyurethane. Additionally, Sánchez-Moreno et al. [25] utilized colloidal nanosilica particles for repairing cracked concrete.

There have not been many attempts to study sealing mortar based on slag. Therefore, there is a need for research on materials that can minimize damage to structures by controlling cracks or wedging supports.

This study focuses on the valorization of blast furnace slag sourced from the Annaba Iron and Steel Plant (Algeria). The aim is to optimize its incorporation into a specialized application: a high-performance sealing mortar for wedging supports and sealing machine bases.

The present work compares three sealing mortar samples: a commercial shrinkage-compensated sealer and two laboratory-formulated sealers, with and without slag.

## 2 Materials and methods

### 2.1 Materials

Three prismatic mortar samples (M10, M234, and MISO) measuring 4 × 4 × 16 cm were prepared. The first sample, M10, is a substitution of 10% of the cement by slag (by weight). The second sample, M234, is a commercial concrete sealer that falls under the category of shrinkage-compensated sealing mortars. The last sample, MISO, is a reference laboratory-made mortar that does not contain granulated blast furnace slag.

The exact composition of M234 is not disclosed by the manufacturer but the product is commonly used as a reference in this field, since our study focuses on performance comparison, not material composition.

The following raw materials (cement, sand, slag, and additives) were combined in a dry state to create a powder that could be hydrated with tap water to form a fluid mixture suitable for manufacturing the mortar samples.

#### 2.1.1 Cement

The clinker used came from Portland Cement (CEM I 42.5 R) from the Meftah cement plant, with a fineness of 4400 $cm^2/g$, a density of 3110 $kg/m^3$, an initial setting time of 150 min, and a final setting time of 240 min, with a water demand of 29%. The chemical and mineralogical composition of the cement is detailed in Tables 1 and 2.

For producing the M10 mortar, the clinker was mixed with 5% gypsum and 10% slag, ground to a fineness of 5150 $cm^2/g$ using a RETSCH PM 200 Planetary Ball Mill.

**Table 1** Chemical composition of Portland Cement used, determined by XRF

| Oxide component wt. (%) | | | | | | | | | |
|---|---|---|---|---|---|---|---|---|---|
| $SiO_2$ | $Al_2O_3$ | $Fe_2O_3$ | CaO | Free CaO | MgO | $Na_2O$ | $K_2O$ | $SO_3$ | Loss Ign. |
| 21.50 | 5.20 | 3.78 | 62.41 | 0.17 | 1.06 | - | 0.66 | 2.73 | 0.81 |

**Table 2** Mineralogical composition of cement (calculated according to the BOGUE formula)

| | $C_3S$ | $C_2S$ | $C_3A$ | $C_4AF$ | CaOF |
|---|---|---|---|---|---|
| Cement minerals (%) | 60.10 | 20.17 | 09.37 | 10.29 | ≤01 |

### 2.1.2 Blast furnace slag

The blast furnace slag used has a moisture content of 10%, is granulated, vitreous, and light grey in color, and was obtained from the Annaba Iron and Steel Plant (Algeria). After grinding in a RETSCH PM 200 planetary mill, it was reduced to an extremely fine powder with a median particle size of 23 µm and a particle size distribution of less than 63 µm. The slag has an absolute density of 2370 kg/m$^3$ and a bulk density of 890 kg/m$^3$. Its chemical composition is shown in Table 3. The particle size of the blast furnace slag was measured using a Laser Particle Size Analyzer, and the results are presented in Fig. 1.

### 2.1.3 Sand

Standardized sand was used and prepared in compliance with standard NA 5043:2024 [28]. The calculated sand equivalent value is ES ≥ 99%. Tables 4 and 5 provide the sand's fineness modulus and the quantity utilized, respectively.

### 2.1.4 Superplasticizer

A white powder from a new generation of superplasticizer was utilized as an additive. It is a non-chlorinated, water-reducing agent based on modified polycarboxylates.

### 2.1.5 Specimen preparation

The preparation of the mortars under study involved mixing cement, sand, and slag in a dry state. A specific water-to-cement weight ratio of 0.42 was maintained. Details on the mix proportioning are presented in Table 6. The amount of cement substitution with slag was 10%. A composition with 0 wt% slag was also prepared as a reference.

## 2.2 Characterization method

### 2.2.1 Study of mortar durability indices

*Capillary absorption*

The capillary absorption test was carried out according to the protocol defined by AFPC-AFREM [29], with additional time periods between 2 and 15 min at early age. Three specimens were used to determine their capillary absorption coefficient. After 28 days of curing, the specimens were oven-dried at 80 °C until a constant weight was achieved. The five sides of the specimens were then sealed with aluminum adhesive paper, leaving the water-absorbing surface unsealed. During this test, the water level was maintained at about 3 mm above the base of the specimens. The initial mass of the specimen was weighed and recorded as $M_0$, and the mass of the specimen at time $t$ was recorded as $M_{x(t)}$. The capillary absorption coefficient is defined

**Table 3** Chemical composition of the blast furnace slag used, determined by XRF

| Oxide component wt. (%) | | | | | | | | | | | | |
|---|---|---|---|---|---|---|---|---|---|---|---|---|
| $SiO_2$ | $Al_2O_3$ | $Fe_2O_3$ | CaO | MgO | $K_2O$ | $TiO_2$ | $Na_2O$ | $SO_3$ | BaO | MnO | SrO | Loss Ign. |
| 41.2 | 8.16 | 0.937 | 39.22 | 3.25 | 1.15 | 0.351 | 0.332 | 1.03 | 0.88 | 2.228 | 0.274 | 0.936 |

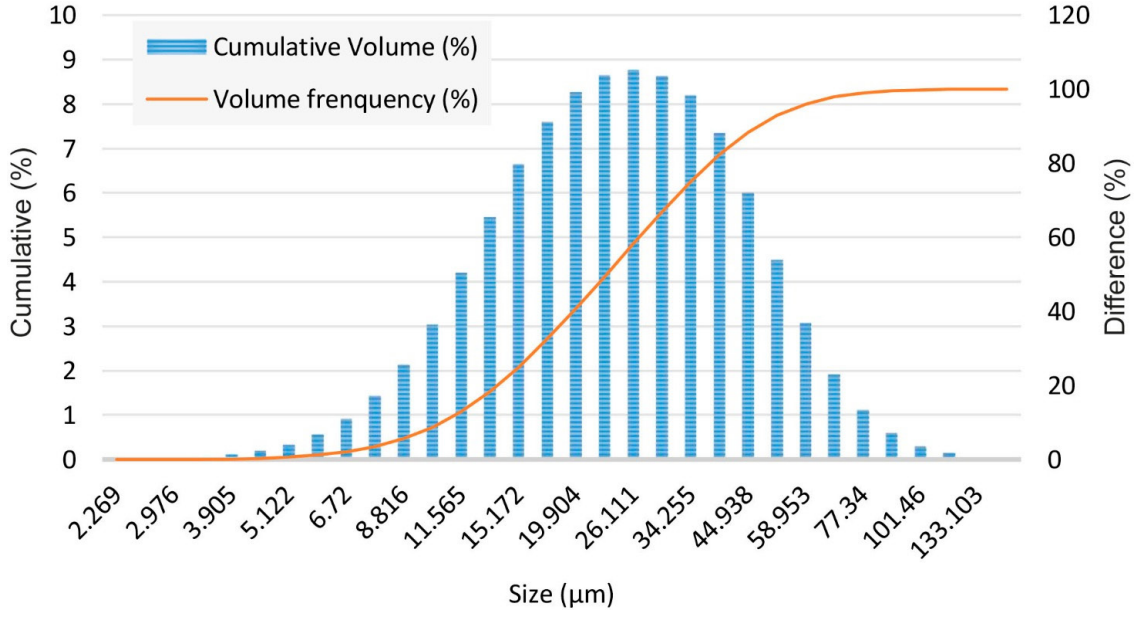


**Fig. 1** Average particle size distribution of blast furnace slag and undersize curve measured

**Table 4** Fineness modulus of the sand

| Sand | Coarse sand (50% coarse + 50% medium) | Fine sand | Preferential sand |
|---|---|---|---|
| Fineness modulus | 3.68 | 0.91 | 2.20 |

**Table 5** Amount of sand used

| Sand | Coarse sand (50% coarse + 50% medium) | | Fine sand | Preferential sand |
|---|---|---|---|---|
| | Coarse sand | Medium sand | | |
| Ratio % | 23.285 | 23.285 | 53.43 | 100 |
| Weight (g) | 314.35 | 314.35 | 721.305 | 1350 |

**Table 6** Mixture proportioning

| Mortar | Cement* (g) | Slag (g) | Sand (g) | Water (ml) | Additives (%) | *W/C* |
|---|---|---|---|---|---|---|
| M ISO | 450 | 0 | 1350 | 189 | 0.2 | 0.42 |
| M 10 | 405 | 45 | 1350 | 189 | 0.2 | 0.42 |

* Cement: 95% Clinker + 5% gypsum

according to Eq. (1) and is used to translate the amount of water absorbed in relation to the surface in contact.

$$C_{a,t} = \frac{M_x - M_0}{A} \quad (1)$$

Where:

- $C_{a,t}$ is the capillary absorption coefficient at time $t$ (kg/m$^2$),
- $M_x$ is the total amount of water absorbed (kg),
- $M_0$ is the initial mass of the specimen,
- $A$ is the cross-sectional area of the specimens in contact with water (0.0016 m$^2$).

*Water accessible porosity*

Water accessible porosity is determined by the absorption of water through immersion, which is the difference between the mass of a sample saturated in water and its mass in the dry state. Three specimens were used for this test, and they were dried at 105 °C to a constant mass with a fluctuation of 0.1% after 24 h. The dry mass of the samples, denoted as $M_{dry}$, was thus determined. The water accessible porosity of the studied specimens was determined using the water saturation method.

To obtain the porosity accessible to water by immersion ($P_W$), the samples were immersed in water until saturation (with a mass variation of 0.1% after 24 h), in accordance with standard (NBN B 15-215:2018 [30]) [31]. The samples were then weighed in air ($M_{sat}$) and in water ($M_{water}$). $P_W$ is defined as the open porosity of the material.

On the other hand, the porosity accessible to water by vacuum immersion ($P_{WV}$) was determined in accordance with standard NBN B 24-213:1976 [32]. This involved saturating the samples in a vacuum and then weighing them in air ($M_{satV}$) and in water ($M_{waterV}$). $P_{WV}$ is defined as the total porosity of the material.

Thus, the porosities $P_W$ and $P_{WV}$ are calculated according to Eq. (2) and Eq. (3), respectively.

$$P_W = \frac{M_{sat} - M_{dry}}{M_{sat} - M_{water}}(\%) \quad (2)$$

$$P_{WV} = \frac{M_{satV} - M_{dry}}{M_{satV} - M_{waterV}}(\%) \quad (3)$$

The closed porosity ($P_c$) can be deduced from the difference between the total porosity ($P_{WV}$) and the open porosity ($P_W$) Eq. (4).

$$P_c = P_{WV} - P_W\,(\%) \quad (4)$$

*Non-steady-state migration coefficient of chloride ion*

The apparent diffusion coefficient of chlorides $D_{nssm}$ is measured by a chloride ion migration test under an electric field in accordance with the procedure described in the standard XP P18-462:2012 [33]. The test is carried out on prismatic sample of dimensions (15 × 5 cm) Fig. 2.

After testing, the specimens are fractured by splitting and sprayed with a solution of silver nitrate ($AgNO_3$) to reveal the penetration front of the chlorine ions.

The silver nitrate whitens the part penetrated by the chlorine ions by forming a white precipitate. The non-steady-state migration coefficient is defined by the Eq. (5).

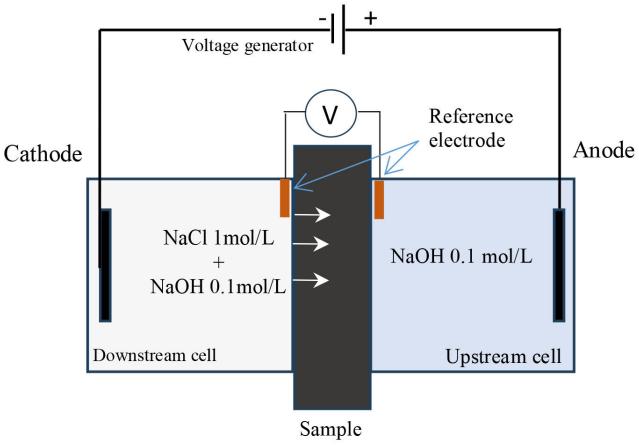


**Fig. 2** Device for accelerated testing of non-steady-state migration coefficient of chloride ion

$$D_{nssm} = \frac{0.0239(273+T)L}{(U+2)t}\left(x_d - 0.0238\sqrt{\frac{(273+T)Lx_d}{U-2}}\right) \times 0.20\left(11.6 - 0.0238\sqrt{16383.61}\right) \quad (5)$$

Where:

- $D_{nssm}$ is the non-steady-state migration coefficient of chloride ion ($\times 10^{-12}$ m$^2$/s);
- $T$ is the average temperature between the start and end of the trial (°C);
- $L$ is the thickness of the sample (mm);
- $U$ is the absolute value of the applied voltage (V);
- $x_d$ is the average value of chloride penetration (mm)
- $t$ is the migration test time (h).

The penetration of chloride ions is one of the main phenomena responsible for the corrosion of reinforcement and the deterioration of reinforced concrete structures. The action of chloride ions is specific to certain environments in which concrete may be found, such as structures in marine environments (submerged parts, tidal zones, surfaces subject to sea spray, etc.) or those exposed to de-icing salts.

### 2.2.2 Measurement of sonic wave propagation time and speed (NA 5027)

The propagation characteristics of ultrasonic waves in a material can reveal valuable information about its properties. For instance, the wave's propagation speed provides insight into the material's microstructure and damage state. This study used the PUNDIT LAB ultrasonic testing equipment, following the measurement procedure specified in the standard NA 5027:2022 [34]. This standard defines the measurement process, which involves recording the travel time of an ultrasonic wave generated by an electroacoustic transducer as it propagates through the mortar. The device, which generates and receives ultrasonic waves digitally, supports piezoelectric transducers within a frequency range of 20 to 500 kHz. Consistent with Gaydecki et al.'s [35] recommendation of using lower frequencies (40–80 kHz) for concrete testing, a frequency of 54 kHz was selected for this investigation. The direct transmission method, deemed the most reliable due to the longitudinal pulses propagating normally to the transducer's face, was utilized. The pulser and receiver were positioned on opposing surfaces of the concrete sample, as illustrated in Fig. 3.

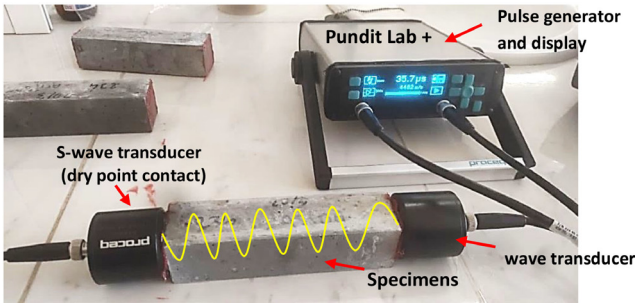


**Fig. 3** Setting up ultrasonic velocity measurement using Pundit Lab+ on prismatic mortar samples (4 × 4 × 16 cm)

Ultrasonic wave velocity in concrete is calculated by dividing the concrete thickness by the travel time. Therefore, the pulse velocity ($V$) can be determined using Eq. (6).

$$V = \frac{L}{t} \quad (6)$$

Where $V$ is the velocity (m/s), $L$ is the distance (m) and $t$ is the time (s).

## 3 Results and discussion

### 3.1 Characterization of fresh mortar

These tests were conducted on the pastes of different mortars to determine the water requirement for normal consistency and setting times in accordance with the standard (NA 230:2019 [36]). The values obtained are presented in Table 7.

The commercial mortar M234, with a spread of 30 cm, exhibits the highest fluidity, indicating a more fluid consistency. In contrast, Grout 234, with a spread of 27 cm, is less fluid but remains flowable, likely due to slightly higher viscosity. The M10 mortar, with the lowest spread of 23 cm, shows the lowest fluidity, indicating the thickest and least flowable consistency. Meanwhile, M ISO, with a spread of 25 cm, falls between M10 and Grout 234, suggesting intermediate flowability.

The finer slag used in the M10 mortar likely increases water demand due to its higher surface area, which reduces workability and results in a lower spread (23 cm).

**Table 7** Characteristics of the studied samples

| Samples | Setting time (min) | | Density (g/l) | Spread (cm) |
|---|---|---|---|---|
| | Start | End | | |
| Grout 234 (fluid consistency) | 240 | 270 | 2390 | 30 |
| Grout 234 (plastic consistency) | 195 | 210 | | 27 |
| M 10 | 200 | 220 | 2132 | 23 |
| M ISO | 270 | 300 | 2064 | 25 |

Finer particles enhance hydration and C-S-H gel formation, leading to increased closed porosity in slag mortars. This, in turn, may raise internal friction and reduce flowability, resulting in lower spread values compared to the reference mortar (free of slag M ISO).

A higher slag content (particularly with finer particles, as in M10) reduces the consistency of fresh mortar, decreasing the spread (e.g., 23 cm for M10 vs. 27–30 cm for Grout 234) and making the mix less fluid and more plastic or stiff. This is primarily due to the increased water demand and the denser microstructure resulting from C-S-H gel formation and greater closed porosity.

CEN EN 445:2007 standard [37] generally specifies a spread of 25–30 cm or higher for injection grouts to ensure adequate flowability. A minimum spread of 27 cm is typically required for effective injection, with 30 cm considered ideal for fine cracks.

In conclusion, increasing the slag content, especially with finer particles (as in M10), decreases the consistency of fresh mortar, resulting in a lower spread (e.g., 23 cm for M10 compared to 27–30 cm for Grout 234). This leads to a stiffer, less fluid mix with a more plastic consistency. The reduced fluidity is attributed to greater water demand, a denser microstructure from C-S-H gel formation, and higher closed porosity.

For effective injection, a spread of 27–30 cm or higher is preferred. Grout 234 (fluid) is ideal, while the plastic variant may be acceptable in less demanding conditions. However, M10 (23 cm) and M ISO (25 cm) are too viscous for most injection purposes.

### 3.2 Characterization of hardened mortar

#### 3.2.1 Mechanical properties

Flexural strength was tested on three prismatic mortar specimens measuring 40 × 40 × 160 mm for each variable, in accordance with the standard (NA 234:2018 [38]) [39]. The prisms resulting from the bending test were then tested in compression on the lateral faces of the mold, under a section of 40 × 40 mm$^2$, also in accordance with NA 234:2018 [38]. Compressive strength is the average of six measurements.

Figs. 4 and 5 show the compressive and flexural strengths in accordance with standard NA 234:2018 [38]. It can be observed that both mortars satisfy the requirements related to the exposure classes for which they were designed. Additionally, M234 mortar exhibits marginally greater compressive and flexural strengths than M10 mortar.

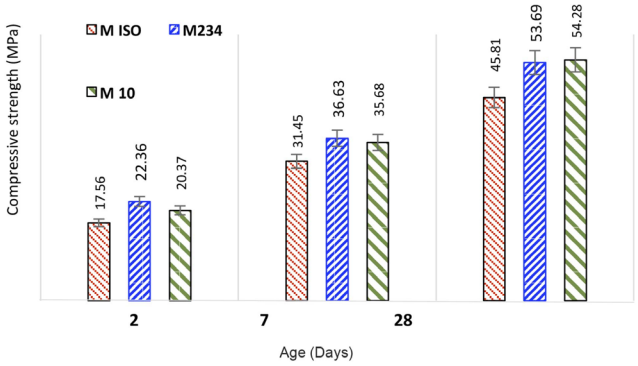


**Fig. 4** Compressive strength (MPa) of mortars at 2, 7 and 28 days of curing

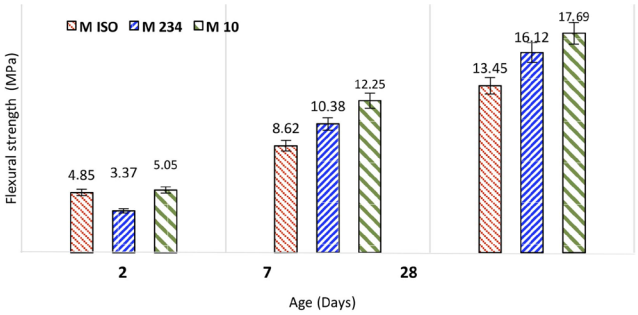


**Fig. 5** Flexural strength (MPa) of mortars at 2, 7 and 28 days of curing

The M10 mortar shows results comparable to those obtained with M234. Literature indicates that mortars based on blast furnace slag generally have higher compressive strengths than those based on CEM I, assuming all other conditions remain constant. This finding is supported by the results of the compressive strength tests. Moreover, the slag from the blast furnace used to make M10 mortar is finer than that used for the commercial mortar M234.

#### 3.2.2 Capillary absorption

Observations of the capillary fringes on the mortar samples show higher absorption kinetics along the resin-insulated faces, with a thickness ranging from 12 to nearly 35 mm, as illustrated in Fig. 6.

Fig. 7 shows that the absorption coefficient of slag mortars is lower than that of the concrete without slag (MISO

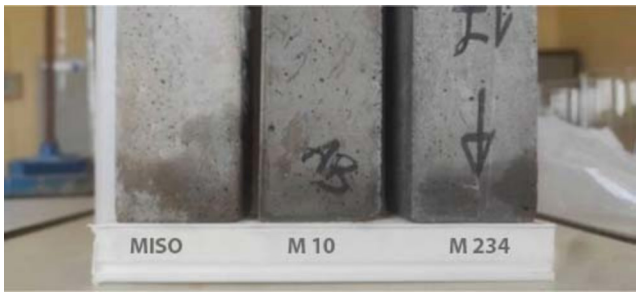


**Fig. 6** Capillary water absorption of Mortar samples

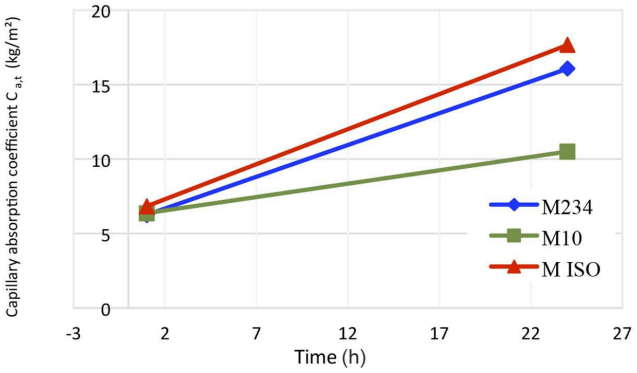


**Fig. 7** The capillary absorption of mortars between 1 and 24 h

sample), which can be explained by the more refined pore structure. The positive effect of slag on the capillary absorption of mortars has been reported in the literature for low percentages of slag [21]. This improvement is attributed to the way in which slag hydration modifies the dimensions and distribution of capillary porosity, leading to the formation of CSH gel [40].

### 3.2.3 Water accessible porosity

The variation in water-accessible porosity ($P_W$) and vacuum water-accessible porosity ($P_{WV}$) of the studied mortars after 28 days of curing is shown in Fig. 8. The straight green line in Fig. 8 represents the closed porosity ($P_c$) for MISO, M234, and M10 mortars.

A higher closed porosity of the slag mortars compared to the reference mortar is observed. However, there is little variation in $P_c$ between M234 and M10. Despite the high porosity, this reflects the discontinuous porous structure of the slag mortars. This variation is typical and results from the latent hydration of the slag in the Portland cement. This is largely confirmed by the mechanical behavior observed two months after curing.

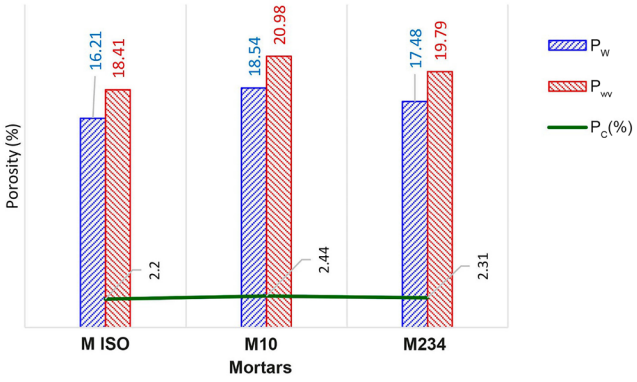


**Fig. 8** Variation in water-accessible porosity $P_W$% and vacuum water-accessible porosity $P_{WV}$ of the studied mortars

The findings logically demonstrate that the mortar with the lowest porosity is the most compact. While the porosity of M234 is the lowest, it is still greater than that of MISO. The fact that mortar M234 contains a considerable amount of blast furnace slag, whereas mortar MISO does not, could explain this difference. Similar results with mortars containing 0–40% blast furnace slag was obtained by [41] and [42].

Jiang et al. [3] showed that the total porosity of mortars based on slag cement is higher than that of mortars made with cement without added additives. However, he found a narrower and finer pore size distribution in slag cement mortars. According to his work, the hydration of slag at a young age is very slow compared to that of clinker. The hydrates formed are mainly primary sulphoaluminate, which occur as dispersed needles, leaving accessible voids.

Over time, the slag is activated by $Ca(OH)_2$ from the hydration of the clinker, forming CSH gel, which fills the structure formed by the ettringite needles. As a result, compared to regular Portland cement, the capillary pore volume is reduced, and the pore structure is finer.

### 3.2.4 Results of non-steady-state migration coefficient of chloride ion

Fig. 9 shows the results obtained from the transient chloride ion migration test on the two M10 and M234 mortars.

The threshold values shown in Fig. 10 are taken from the AFGC guide [29]. It can be seen that both mortars have an apparent diffusion coefficient between 1.74 and 2.09 × $10^{-12}$ $m^2/s$, thus falling within the high potential durability class. Although the M10 mortar has a lower chloride ion diffusion coefficient than the compact M234, the composition of the binder has a significant impact on the apparent chloride ion diffusion coefficient. These results are consistent with the literature, which shows that concretes containing blast furnace slag can bind more chloride ions than mortars based on Portland cement [43] and, due to their finer porosity [44], have a lower chloride ion diffusion coefficient than MISO.

### 3.2.5 Results of propagation of ultrasonic waves

The results obtained for the three mortars studied are presented in Fig. 11. The measurements were taken on hardened specimens that were kept under wet curing conditions.

The results for the propagation speed of sonic waves indicate that the three mortars are classified as very high-strength mortars according to the RILEM curve [45]. This

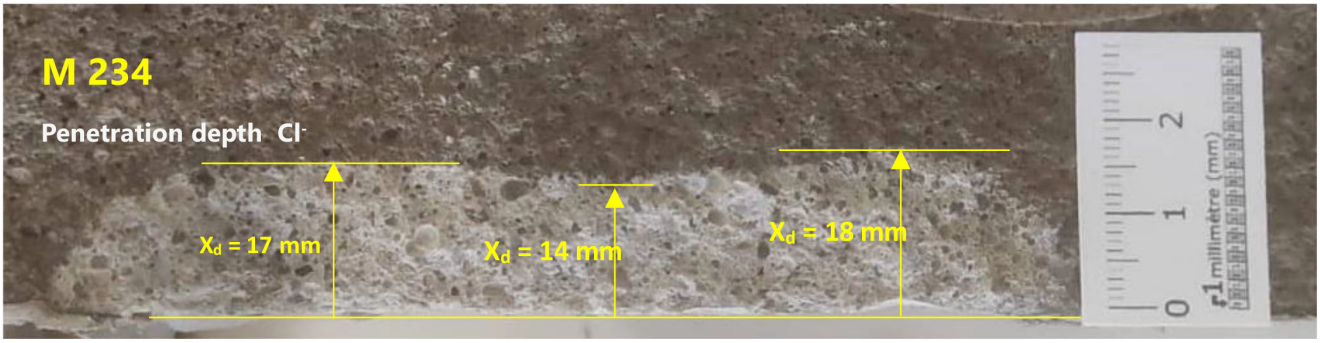


(a)

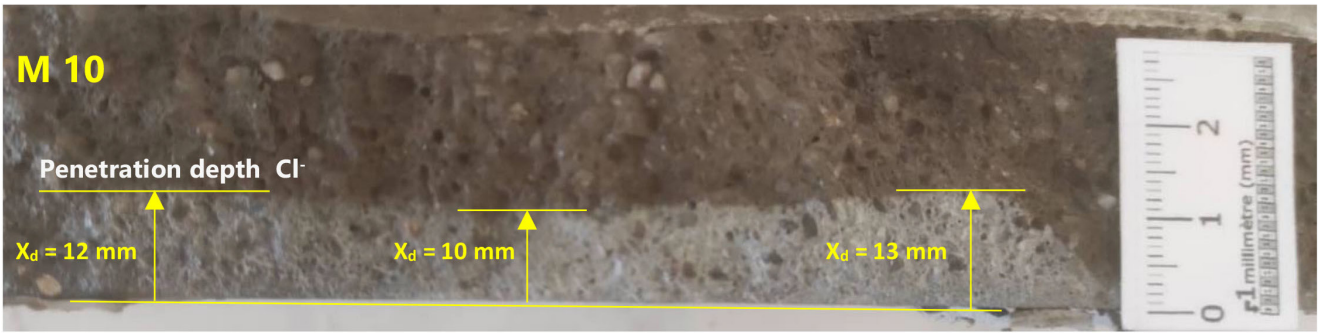


(b)

**Fig. 9** Mortar fracture after chlorine ion diffusion test and silver nitrate spraying: (a) M234 Mortar, (b) M10 Mortar

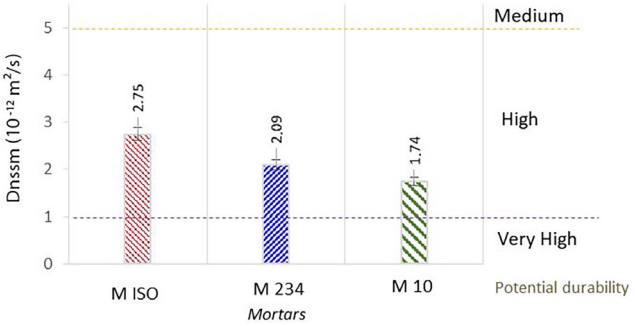


**Fig. 10** Apparent diffusion coefficient on chloride-activated mortar obtained by non-steady-state migration test with indication of potential durability according to the guide AFGC [29]

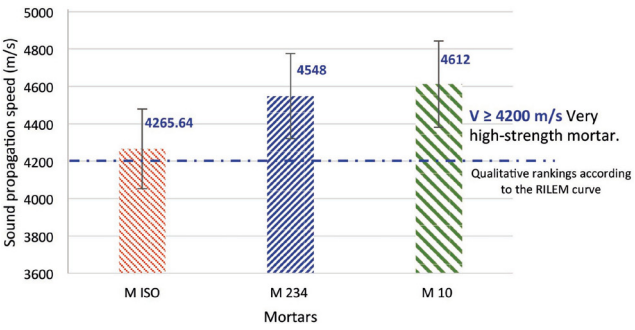


**Fig. 11** Sound wave propagation speed of three mortars according to standard

classification also supports the findings related to porosity and mechanical strength.

Fig. 11 shows that the speed of propagation of ultrasonic waves increases with the addition of blast-furnace slag to the mortar. This is because blast-furnace slag powder acts as a filler, reducing porosity and aiding the cement hydration process, which makes the test specimen denser. As the density of the specimen increases, the medium through which the ultrasonic waves propagate becomes more confined, resulting in an increase in the measured wave speed.

The Ultrasonic Pulse Velocity (UPV) test measures the transit time of ultrasonic pulses at 54 kHz, generated by an electroacoustic transducer and passing from one surface of the specimen to the other. The transit time of the ultrasonic pulses depends on the density and elastic properties of the material being tested.

Fig. 12 presents the transit time of ultrasonic pulses for three mortars (MISO, M234, and M10), measured at 54 kHz. The data reveals that the signal curve for the reference mortar (MISO) displays a distinct and consistent pattern of ultrasonic pulses, with a noticeably shorter transit time compared to the other two mortars. Typically, shorter ultrasonic pulse transit times are associated with denser, more uniform materials that have stronger particle bonds. This is because denser materials exhibit higher ultrasonic pulse velocities, as they provide greater resistance to wave propagation, which in turn accelerates the pulse's travel [46, 47]. The density and elastic modulus of

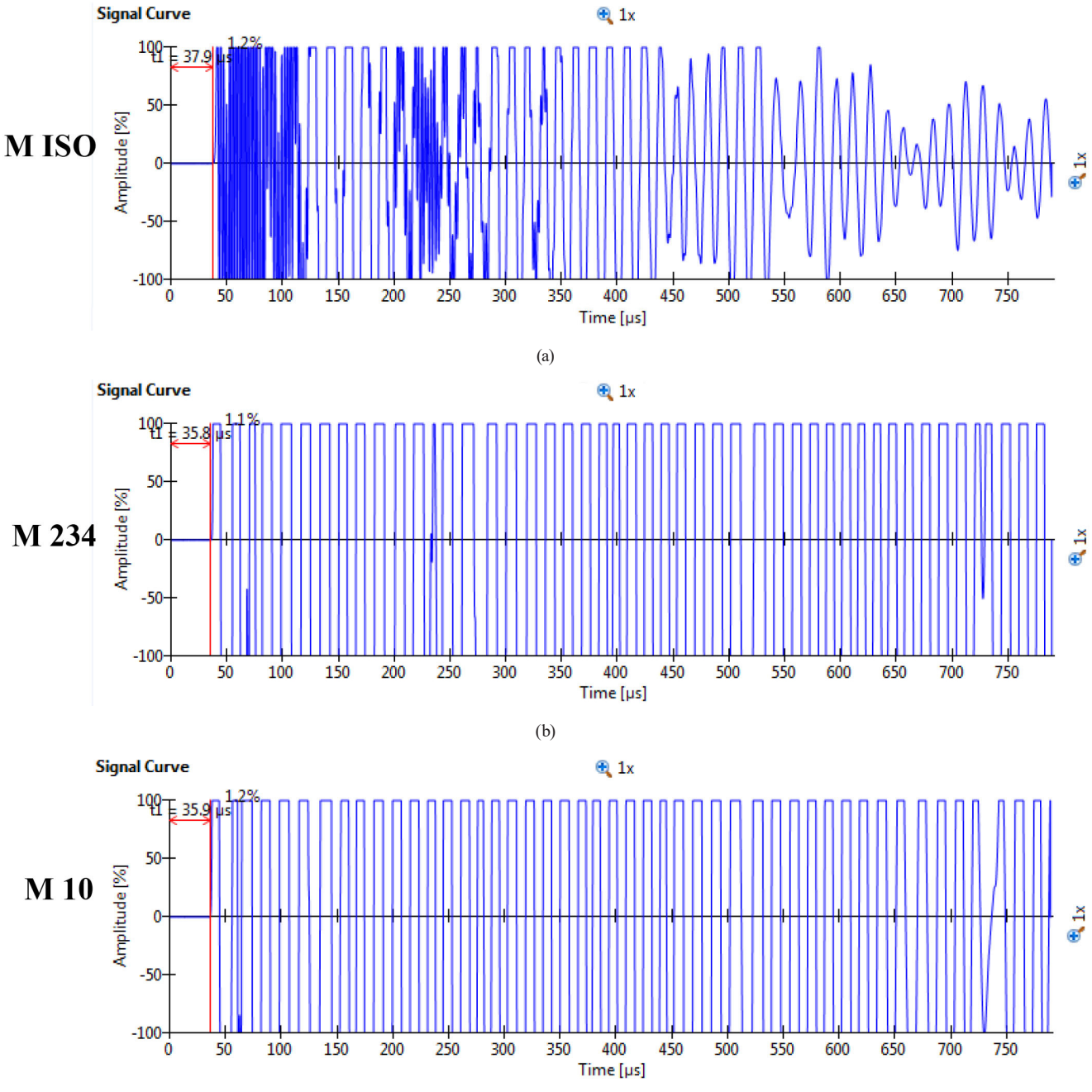


**Fig. 12** Transit time of ultrasonic pulses with 54 kHz of mortars tested: (a) MISO, (b) M234, (c) M10

concrete influence the speed at which ultrasonic pulses travel through it. In other words, faster-moving ultrasonic pulses are indicative of denser and stiffer materials [48].

In contrast to the M234 and M10 mortars, the signal curve of MISO exhibits a less defined and more irregular pattern. Additionally, the transit time appears to be significantly longer compared to that of MISO. Since GGBS hydrates more slowly than the primary binder phases in cement, it may leave some unreacted particles and create more voids, which could initially result in increased porosity. This effect may be due to the higher proportion of GGBS in this concrete. However, the continued hydration of GGBS can eventually fill these voids, reducing overall porosity and improving long-term strength and durability [49]. Porosity or void spaces in concrete, can prevent the propagation of ultrasonic vibrations. As the waves are attenuated more when traveling through these voids, concrete with higher porosity typically shows lower ultrasonic pulse velocities [47].

Moreover, we observe that the ultrasonic pulse velocities of the three mortars MISO, M234, and M10 are 4223 m/s, 4471 m/s, and 4459 m/s, respectively. These values are within the normal range, as the ultrasonic pulse velocity of undamaged concrete typically varies between 3000 and 4500 m/s [50]. Loke et al. [51] found that increasing GGBS content in mortar tends to decrease the UPV values compared to conventional cement-based mortar, and this result was attributed to the slower setting and hardening behavior of GGBFS compared to ordinary cement.

## 4 Conclusions

In this study, a commercial sealing mortar was characterized to compare its performance with two laboratory-made concrete sealers, which were formulated by substituting cement with blast furnace slag. Based on the materials and measurement methods used in this paper, the following conclusions can be drawn:

- Granulometry showed that a particle size of less than 63 μm was achieved for the slag after grinding.
- The M10 mortar demonstrated results comparable to those obtained with M234; notably, the blast furnace slag used in M10 is finer than that used to prepare the commercial mortar M234.
- The positive effect of slag on the capillary absorption of mortars was attributed to the modification of capillary porosity dimensions and distribution caused by slag hydration, resulting in the formation of C-S-H gel.
- A higher closed porosity of the slag mortars compared to the reference mortar (MISO) was observed, reflecting the discontinuous porous structure of the slag mortars.
- Capillary water absorption tests showed that the absorption coefficient of slag mortars is lower than that of the concrete without slag (MISO sample), which can be explained by the more refined pore structure.
- The speed of propagation of sonic waves indicated that the three mortars are classified as very high-strength mortars.

## References

[1] Bulatbekova, D., Vashistha, P., Kim, H.-K., Pyo, S. "Effects of basic-oxygen furnace, electric-arc furnace, and ladle furnace slags on the hydration and durability properties of construction materials: A review", Journal of Building Engineering, 92, 109670, 2024. https://doi.org/10.1016/j.jobe.2024.109670

[2] Yildirim, I. Z., Prezzi, M. "Steel slag: chemistry, mineralogy, and morphology", In: IFCEE 2015, San Antonio, TX, USA, 2015, pp. 2816–2825. ISBN 9780784479087 https://doi.org/10.1061/9780784479087.263

[3] Jiang, Y., Ling, T.-C., Shi, C., Pan, S.-Y. "Characteristics of steel slags and their use in cement and concrete—A review", Resources, Conservation and Recycling, 136, pp. 187–197, 2018. https://doi.org/10.1016/j.resconrec.2018.04.023

[4] Ibrahim, M. H., El-Naas, M. H., Benamor, A., Al-Sobhi, S. S., Zhang, Z. "Carbon mineralization by reaction with steel-making waste: A review", Processes, 7(2), 115, 2019. https://doi.org/10.3390/pr7020115

[5] Holappa, L., Kekkonen, M., Jokilaakso, A., Koskinen, J. "A review of circular economy prospects for stainless steelmaking slags", Journal of Sustainable Metallurgy, 7(3), pp. 806–817, 2021. https://doi.org/10.1007/s40831-021-00392-w

[6] Gencel, O., Musatat, A. B., Demir, A., Tozluoğlu, A., Tutuş, A., Kıllı, U., Fidan, H., Kosovalı Cavuş, F. "Transforming industrial byproduct to eco-friendly functional material: Ground-granulated blast furnace slag reinforced paper for renewable energy storage", Science of The Total Environment, 954, 176616, 2024. https://doi.org/10.1016/j.scitotenv.2024.176616

[7] Matthes, W., Vollpracht, A., Villagrán, Y., Kamali-Bernard, S., Hooton, D., Gruyaert, E., Soutsos, M., De Belie, N. "Ground granulated blast-furnace slag", In: De Belie, N., Soutsos, M., Gruyaert, E. (eds.) Properties of Fresh and Hardened Concrete Containing Supplementary Cementitious Materials: State-of-the-Art Report of the RILEM Technical Committee 238-SCM, Working Group 4, Springer, 2017, pp. 1–53. ISBN 978-3-319-70605-4 https://doi.org/10.1007/978-3-319-70606-1_1

[8] Samantasinghar, S., Singh, S. P. "Fresh and hardened properties of fly ash–slag blended geopolymer paste and mortar", International Journal of Concrete Structures and Materials, 13(1), 47, 2019. https://doi.org/10.1186/s40069-019-0360-1

[9] Arivalagan, S. "Sustainable studies on concrete with GGBS as a replacement material in cement", Jordan Journal of Civil Engineering, 8(3), pp. 263–270, 2014.

[10] Sardar, S., Joshi, D. A. "Comparative study of GGBS concrete with OPC concrete for assessment of $CO_2$ emission reduction and cost saving", [pdf] International Journal of Technical Innovation in Modern Engineering & Science, 4(10), pp. 353–356, 2018. Available at: https://www.ijtimes.com/index.php/ijtimes/article/view/544/504

[11] International Conference on Recent Advancements in Civil Engineering, Thomas, G. E., Indira, P. V., Sajith, A. S. "Enhancement of mechanical properties of cement mortar using ground granulated blast furnace slag as a partial replacement", In: Recent Trends in Civil Engineering: Select Proceedings of ICRACE 2021, Silchar, India, 2023, pp. 171–180. ISBN 978-981-19-4054-5 https://doi.org/10.1007/978-981-19-4055-2_15

[12] Tan, Y., Tang, K. "Modelling in situ concrete temperature development: the impact of ambient temperature and GGBS replacement", CivilEng, 5(3), pp. 694–716, 2024. https://doi.org/10.3390/civileng5030037

[13] Richardson, A. E., Walker, S. L., Hart, A. "Comparative thermal performance test for GGBS and OPC concrete mixes", [pdf] presented at Ecozoom: International Conference on Sustainability in Building, Aarhus, Denmark, Nov., 25, 2009. Available at: https://core.ac.uk/download/4148155.pdf

[14] Ahmad, J., Kontoleon, K. J., Majdi, A., Naqash, M. T., Deifalla, A. F., Ben Kahla, N., Isleem, H. F., Qaidi, S. M. "A comprehensive review on the ground granulated blast furnace slag (GGBS) in concrete production", Sustainability, 14(14), 8783, 2022. https://doi.org/10.3390/su14148783

[15] Cahyani, R. A. T., Rusdianto, Y. "Concrete performance with ground granulated blast furnace slag as supplementary cementitious materials", IOP Conference Series: Materials Science and Engineering, 771(1), 012062, 2020. https://doi.org/10.1088/1757-899X/771/1/012062

[16] Parron-Rubio, M. E., Perez-Garcia, F., Gonzalez-Herrera, A., Oliveira, M. J., Rubio-Cintas, M. D. "Slag substitution as a cementing material in concrete: Mechanical, physical and environmental properties", Materials, 12(18), 2845, 2019. https://doi.org/10.3390/ma12182845

[17] Jacobson, A. "Granulated Blast Furnace Slag and its Effects on Concrete Mixes", BS in Construction Management, College of Architecture and Environmental Design, 2021. [online] Available at: https://digitalcommons.calpoly.edu/cmsp/515

[18] Liu, Y., Su, Y., Xu, G., Chen, Y., You, G. "Research progress on controlled low-strength materials: metallurgical waste slag as cementitious materials", Materials, 15(3), 727, 2022. https://doi.org/10.3390/ma15030727

[19] Monshi, A., Asgarani, M. K. "Producing Portland cement from iron and steel slags and limestone", Cement and Concrete Research, 29(9), pp. 1373–1377, 1999. https://doi.org/10.1016/S0008-8846(99)00028-9

[20] Tsakiridis, P. E., Papadimitriou, G. D., Tsivilis, S., Koroneos, C. "Utilization of steel slag for Portland cement clinker production", Journal of Hazardous Materials, 152(2), pp. 805–811, 2008. https://doi.org/10.1016/j.jhazmat.2007.07.093

[21] Vejmelková, E., Pavlíková, M., Keršner, Z., Rovnaníková, P., Ondráček, M., Sedlmajer, M., Černý, R. "High performance concrete containing lower slag amount: A complex view of mechanical and durability properties", Construction and Building Materials, 23(6), pp. 2237–2245, 2009. https://doi.org/10.1016/j.conbuildmat.2008.11.018

[22] Wang, Q., Yan, P., Yang, J., Zhang, B. "Influence of steel slag on mechanical properties and durability of concrete", Construction and Building Materials, 47, pp. 1414–1420, 2013. https://doi.org/10.1016/j.conbuildmat.2013.06.044

[23] Teng, S., Lim, T. Y. D., Sabet Divsholi, B. "Durability and mechanical properties of high strength concrete incorporating ultra fine ground granulated blast-furnace slag", Construction and Building Materials, 40, pp. 875–881, 2013. https://doi.org/10.1016/j.conbuildmat.2012.11.052

[24] Muhammad, N. Z., Keyvanfar, A., Abd. Majid, M. Z., Shafaghat, A., Mirza, J. "Waterproof performance of concrete: A critical review on implemented approaches", Construction and Building Materials, 101, pp. 80–90, 2015. https://doi.org/10.1016/j.conbuildmat.2015.10.048

[25] Sánchez-Moreno, M., García-Calvo, J. L., Tavares-Pinto, F. "Colloidal nanosilica treatments for sealing cracks in mortar", Materials, 15(18), 6338, 2022. https://doi.org/10.3390/ma15186338

[26] Issa, C. A., Debs, P. "Experimental study of epoxy repairing of cracks in concrete", Construction and Building Materials, 21(1), pp. 157–163, 2007. https://doi.org/10.1016/j.conbuildmat.2005.06.030

[27] Abolfazli, M., Bazli, M., Heydari, H., Fahimifar, A. "Investigating the effects of cement and polymer grouting on the shear behavior of rock joints", Polymers, 14(6), 1229, 2022. https://doi.org/10.3390/polym14061229

[28] IANOR "NA 5043:2024 Granulats. Éléments de définition, conformité et codification" (NA 5043:2024 Particle size distribution of aggregates), Algerian Institute of Standardization, Algiers, Algeria, 2024. (in French)

[29] Groupe de travail Durabilité des bétons "Essai de carbonatation accélérée, Mesure de l'épaisseur de béton carbonaté, Mode opératoire recommandé par l'AFREM" (Accelerated Carbonation Test, Measurement of Carbonated Concrete Thickness, Operating Procedure Recommended by AFREM), In: Compte-rendu des journees techniques [de l'] AFPC-AFREM, [Groupe de travail] Durabilité des bétons: méthodes recommandées pour la mesure des grandeurs associées à la durabilité, INSA, 1997, pp. 153–158. ISBN 978-2-87649-022-2 (in French)

[30] NBN "NBN B 15-215:2018 Essais sur béton durci - Absorption d'eau par immersion" (NBN B 15-215:2018 Testing hardened concrete - Absorption of water by immersion), Belgian Standards Body, Brussels, Belgium, 2018. (in French)

[31] European Commission "Commission Directive 92/69/EEC of 31 July 1992 adapting to technical progress for the seventeenth time Council Directive 67/548/EEC on the approximation of laws, regulations and administrative provisions relating to the classification, packaging and labelling of dangerous substances", [online] Available at: https://eur-lex.europa.eu/legal-content/EN/TXT/?qid=1760962103234&uri=CELEX%3A31992L0069

[32] NBN "NBN B 24-213:1976 Essais des matériaux de maçonnerie – Absorption d'eau sous vide" (NBN B 24-213:1976 Masonry units testing – Water absorption under vacuum), Belgian Standards Body, Brussels, Belgium, 1976. (in French)

[33] AFNOR "XP P18-462:2012 Essai sur béton durci - Essai accéléré de migration des ions chlorure en régime non-stationnaire - Détermination du coefficient de diffusion apparent des ions chlorure" (Testing hardened concrete - Chloride ions migration accelerated test in non-steady-state conditions - Determining the apparent chloride ions diffusion coefficient), French Standardization Association, Saint-Denis, France, 2012. (in French)

[34] IANOR "NA 5027:2022 Essais pour béton dans les structures – Détermination de la vitesse de propagation des ultrasons (NA 5027:2022 Tests for concrete in structures – Determination of the propagation velocity of ultrasonic pulses), Algerian Institute of Standardization, Algiers, Algeria, 2022. (in French)

[35] Gaydecki, P. A., Burdekin, F. M., Damaj, W., John, D. G. "The propagation and attenuation of medium-frequency ultrasonic waves in concrete: a signal analytical approach", Measurement Science and Technology, 3(1), 126, 1992. https://doi.org/10.1088/0957-0233/3/1/018

[36] IANOR "NA 230:2019 Méthodes d'essais des ciments - Détermination du temps de prise et de la stabilité" (NA 230:2019 Methods for testing cements - Determination of setting time and stability), Algerian Institute of Standardization, Algiers, Algeria, 2019. (in French)

[37] CEN "CEN EN 445:2007 Grout for prestressing tendons – Test methods", European Committee for Standardization, Brussels, Belgium, 2007.

[38] IANOR "NA 234:2018 Méthodes d'essais des ciments - Détermination des résistances mécaniques" (NA 234:2018 Test methods for cement - Determination of mechanical strengths), Algerian Institute of Standardization, Algiers, Algeria, 2018. (in French)

[39] CEN "CEN EN 196-1:2005 Methods of testing cement - Part 1: Determination of strength", Eropean Committee for Standardization, Brussels, Belgium, 2005.

[40] Shi-Ping, J., Grandet, J. "Evolution comparee des porosites des mortiers de ciment au laitier et des mortiers de ciment portland" (Comparative evolution of the porosities of slag cement mortars and Portland cement mortars), Cement and Concrete Research, 19(3), pp. 487–496, 1989. (in French) https://doi.org/10.1016/0008-8846(89)90037-9

[41] Deboucha, W., Leklou, N., Khelidj, A., Pertue, A., Oudjit, M. N. "L'effet du laitier de haut fourneau sur la porosité du mortier" (The effect of blast furnace slag on the porosity of mortar), Academic Journal of Civil Engineering, 35(1), pp. 190–193, 2020. (in French) https://doi.org/10.26168/ajce.35.1.46

[42] Schmitt, L. "Durabilité des ouvrages en béton soumis à la corrosion: optimisation par une approche probabiliste" (Durability of concrete structures subjected to corrosion: optimization by a probabilistic approach), PhD Thesis, INSA de Toulouse, 2019. (in French)

[43] Dhir, R. K., El-Mohr, M. A. K., Dyer, T. D. "Chloride binding in GGBS concrete", Cement and Concrete Research, 26(12), pp. 1767–1773, 1996. https://doi.org/10.1016/S0008-8846(96)00180-9

[44] Khan, M. I. "Nanostructure and microstructure of cement concrete incorporating multicementitious composites", Transportation Research Record: Journal of the Transportation Research Board, 2141(1), pp. 21–27, 2010. https://doi.org/10.3141/2141-05

[45] Bažant, Z. P., Kazemi, M. T. "Size dependence of concrete fracture energy determined by RILEM work-of-fracture method", International Journal of Fracture, 51(2), pp. 21–27, 2010. https://doi.org/10.1007/BF00033974

[46] Wightman, W. E., Jalinoos, F., Sirles, P., Hanna, K. "Application of geophysical methods to highway related problems", [pdf] Federal Highway Administration, Washington, DC, USA, Rep. FHWA-IF-04-021, 2004. Available at: https://rosap.ntl.bts.gov/view/dot/49856/dot_49856_DS1.pdf

[47] Kumar, P., Singh, B. N. "Non-destructive testing of concrete", New Age International, New Delhi, India, 2012.

[48] Aghaei, H., Penkov, G. M., Solomoichenko, D. A., Toorajipour, A., Petrakov, D. G., Jafarpour, H., Ghosh, S. "Density-dependent relationship between changes in ultrasonic wave velocities, effective stress, and petrophysical-elastic properties of sandstone", Ultrasonics, 132, 106985, 2023. https://doi.org/10.1016/j.ultras.2023.106985

[49] Gao, D., Meng, Y., Yang, L., Tang, J., Lv, M. "Effect of ground granulated blast furnace slag on the properties of calcium sulfoaluminate cement", Construction and Building Materials, 227, 116665, 2019. https://doi.org/10.1016/j.conbuildmat.2019.08.046

[50] ASTM "ASTM C 597-16 Standard test method for pulse velocity through concrete", ASTM International, West Conshohocken, PA, USA, 2016. https://doi.org/10.1520/C0597-16

[51] Loke, C. K., Lehane, B., Aslani, F., Majhi, S., Mukherjee, A. "Non-Destructive evaluation of mortar with ground granulated blast furnace slag blended cement using ultrasonic pulse velocity", Materials, 15(19), 6957, 2022. https://doi.org/10.3390/ma15196957